Interaction of the sorting nexin 25 homologue Snazarus with Rab11 balances endocytic and secretory transport and maintains the ultrafiltration diaphragm in nephrocytes

Tamás Maruzs[a,†,*], Dalma Feil-Börcsök[a,b,†], Enikő Lakatos[a,b], Gábor Juhász[a], András Blastyák[a], Dávid Hargitai[c], Steve Jean[c,d], Péter Lőrincz[c], and Gábor Juhász[a,c,*]

[a]Institute of Genetics, Biological Research Centre, Eötvös Loránd Research Network, Szeged, H-6726 Hungary; [b]Doctoral School of Biology, University of Szeged, Szeged, H-6726 Hungary; [c]Department of Anatomy, Cell and Developmental Biology, Eötvös Loránd University, Budapest, H-1117 Hungary; [d]Department of Anatomy and Cell Biology, University of Sherbrooke, Sherbrooke, J1E 4K8 Canada

ABSTRACT **Proper balance of exocytosis and endocytosis is important for the maintenance of plasma membrane lipid and protein homeostasis. This is especially critical in human podocytes and the podocyte-like *Drosophila* nephrocytes that both use a delicate diaphragm system with evolutionarily conserved components for ultrafiltration. Here, we show that the sorting nexin 25 homologue Snazarus (Snz) binds to Rab11 and localizes to Rab11-positive recycling endosomes in *Drosophila* nephrocytes, unlike in fat cells where it is present in plasma membrane/lipid droplet/endoplasmic reticulum contact sites. Loss of Snz leads to redistribution of Rab11 vesicles from the cell periphery and increases endocytic activity in nephrocytes. These changes are accompanied by defects in diaphragm protein distribution that resemble those seen in Rab11 gain-of-function cells. Of note, co-overexpression of Snz rescues diaphragm defects in Rab11 overexpressing cells, whereas *snz* knockdown in Rab11 overexpressing nephrocytes or simultaneous knockdown of *snz* and *tbc1d8b* encoding a Rab11 GTPase-activating protein (GAP) leads to massive expansion of the lacunar system that contains mislocalized diaphragm components: Sns and Pyd/ZO-1. We find that loss of Snz enhances while its overexpression impairs secretion, which, together with genetic epistasis analyses, suggest that Snz counteracts Rab11 to maintain the diaphragm via setting the proper balance of exocytosis and endocytosis.**

Monitoring Editor
Avital Rodal
Brandeis University

Received: Sep 19, 2022
Revised: Jun 5, 2023
Accepted: Jun 6, 2023

INTRODUCTION

Eukaryotic cells contain a remarkably complex endomembrane system consisting of numerous membrane-bound organelles. Continuous, directed flow of material through this system is a prerequisite of normal cell function and is primarily achieved by vesicle-mediated transport. In the case of endocytosis, extracellular material is enwrapped by portions of the plasma membrane (PM). The resulting endocytic vesicles fuse to form early endosomes (EEs), which then mature into late endosomes (LEs). During endosomal maturation, portions of the endosomal membrane and its integral membrane proteins are sorted into the intraluminal vesicles of LEs/multivesicular bodies and are forwarded toward lysosomes where degradation takes place (Huotari and Helenius, 2011). Notably, a significant portion of transmembrane proteins is targeted from the endosomes back to the PM either directly (through the so-called fast recycling pathway) or indirectly through the recycling endosomal compartment (slow recycling pathway) (Naslavsky and Caplan, 2018). Proper functioning of the endocytic and endosomal recycling routes is essential for establishing a steady-state proteome of

This article was published online ahead of print in MBoC in Press (http://www.molbiolcell.org/cgi/doi/10.1091/mbc.E22-09-0421 on June 14, 2023).

†These authors contributed equally to the work.

*Address correspondence to: Tamás Maruzs (maruzs.tamas@brc.hu); Gábor Juhász (juhasz.gabor@brc.hu).

Abbreviations used: dMAPPER, Drosophila membrane-attached peripheral ER; EE, early endosome; LD, lipid droplet; LE, late endosome; ND, nephrocyte diaphragm; RE, recycling endosome; SG, salivary gland.

integral membrane proteins in the PM and for dynamic remodeling in response to changing physiological conditions. Generating vesicles that bud from the donor membrane with a specific content, moving them through the cytoplasm and ensuring their fusion exclusively with the appropriate target organelle all play key roles in this complex system. These processes are driven by proteins and multiprotein complexes and defect of any of these factors (e.g., due to mutations) leads to compromised cell function and the pathogenesis of severe diseases such as cancer and neurodegeneration.

Sorting nexin (Snx) proteins belong to the PX (phox homology)-domain containing protein family that has almost 50 members in humans (Teasdale and Collins, 2012). Besides their common phophoinositide-binding PX-domain that enables their membrane recruitment, different subgroups of Snx proteins contain various other domains that define their further molecular interactions. Many Snx proteins have well-characterized roles in the endosomal system as parts of the retromer complex, while other members of the family have retromer-independent functions (Gallon and Cullen, 2015). Among the latter group, the SNX13/SNX14/SNX19/SNX25 subgroup of mammalian Snx proteins is characterized by a unique domain structure consisting of two predicted N-terminal transmembrane regions, followed by the PXA-RGS-PX-PXC domains (for simplicity, these proteins hereafter will be referred to as Snx-TM proteins). Snx-TM proteins are also involved in different human diseases (Teasdale and Collins, 2012). Among these, the effects of SNX14 mutations are extensively investigated as they lead to a distinct type of cerebellar ataxia syndrome with features of cerebellar atrophy (due to the loss of Purkinje cells), intellectual disability, and coarse facial features (Thomas *et al.*, 2014; Akizu *et al.*, 2015). A recent study showed that SNX14 is a part of endoplasmic reticulum (ER)—lipid droplet (LD) contact sites promoting the incorporation of fatty acids into triacyl-glycerol in mammalian cells (Datta *et al.*, 2019, 2020). Other members of the Snx-TM subgroup also function at contact sites from yeast to mammals and a growing body of evidence points to their involvement in human diseases (Jacques *et al.*, 2005; Bare *et al.*, 2007; Li *et al.*, 2014; Olsson *et al.*, 2014; Henne *et al.*, 2015; Hariri *et al.*, 2019).

The fruit fly *Drosophila melanogaster* has a single Snx-TM protein (encoded by the *CG1514* gene) that is most closely related to human SNX25. The first study about *CG1514* reported the massive expression of this gene in larval fat bodies and described the life span extending effect of loss-of-function (LOF) mutations (Suh *et al.*, 2008); that is why the authors named this gene ***s**orting **n**exin **lazarus**, snazarus* (*snz*). The first molecular function of Snz was recently demonstrated: Snz is involved in normal LD distribution and lipid transport in larval fat body cells, through maintaining triorganellar membrane contact sites between the ER, the PM, and peripheral LDs (Ugrankar *et al.*, 2019). Recently, Snz has also been identified as a regulator of autophagic flux in the fat tissue (Lauzier *et al.*, 2022).

Here, we report a novel function of Snz in larval garland nephrocytes, the highly endocytic, podocyte-like cells of *Drosophila* (Helmstädter *et al.*, 2017). Garland nephrocytes are spherical cells that continuously take up material from the hemolymph and display a highly organized endosomal system (Denholm and Skaer, 2009). Loss of *snz* leads to prominent morphological and functional changes in the endomembrane system of nephrocytes. These include up-regulation of endocytosis, redistribution of recycling endosomes (REs), and alterations of the nephrocyte diaphragm (ND). We show that the effects of *snz* loss are linked to its role in Rab11-dependent recycling and are independent of ER-PM-LD contact sites in this cell type. We propose a model in which Snz negatively regulates exocytosis downstream of Rab11, thus contributing to the maintenance of membrane balance in the endosomal system of nephrocytes.

RESULTS

Loss of Snz enhances endocytic activity in nephrocytes

Labeling endosomal subpopulations is a relatively simple method that gives an overview about endosomal maturation in nephrocytes (Lőrincz *et al.*, 2016). We evaluated the effect of *snz* LOF in nephrocytes by colabeling Rab5 and Rab7 to identify EEs and LEs, respectively. We knocked down *snz* in nephrocytes of wandering-stage larvae by using two independent UAS RNAi lines driven by prospero-Gal4 (Bechtel *et al.*, 2013). In wild-type cells (Figure 1A), EEs and LEs form separate layers in the cytoplasm of the cells. Beneath the PM, small Rab5-positive EEs are formed and then they mature into large, Rab7-positive LEs as they move deeper into the cells. We detected a striking increase in the size of LEs as a result of *snz* knockdown in case of both RNAi lines (Figure 1, B and C). Compared with control cells, nephrocytes expressing *snz* RNAi 1 or *snz* RNAi 2 contain significantly larger LEs, with 2.23 μm^2 mean area in the control versus 4.89 μm^2 and 3.52 μm^2 mean area in the case of RNAi 1 and RNAi 2 knockdowns, respectively. We used the *snz* RNAi 1 line in our further experiments and hereafter we will refer to it as *snz* knockdown. Importantly, *snz* null mutant nephrocytes also contain abnormally enlarged LEs (Figure 1D), and this phenotype can be rescued by the expression of a full-length, C-terminally GFP-tagged Snz fusion protein that restores LE size from 4.25 μm^2 mean area of the mutant to 2.29 μm^2 in the rescue (Figure 1, E and F). Notably, the population of EEs also shows an expansion in *snz* LOF cells (Figure 1, A–E and G). Ultrastructural analysis also confirmed the presence of enlarged LEs in *snz* knockdown cells (Figure 1, H and I). These results show that *snz* loss leads to severe alterations in the main endosomal compartments of nephrocytes.

Next, we carried out ex vivo tracer uptake experiments to assess the functional consequences of the morphological changes detected in the endosomal system of *snz* LOF cells. Live nephrocytes were pulse-labeled with BSA-Alexa Fluor 647 conjugate (hereafter referred to as BSA^{647}) and then fixed after allowing the cells to internalize the tracer during the chase. To evaluate the kinetics of earlier steps of endocytosis, we applied 1-min pulse, followed by a 9-min chase interval. We quantified the amount of the tracer in the subcortical endosomal population, as during this relatively short chase it does not access the perinuclearly located lysosomes. To determine tracer amounts, we considered both the endosomal volume (how much space the tracer molecules fill) and the concentration of the tracer (how many tracer molecules are present in a given space). For this, we quantified the tracer-positive area as well as mean fluorescence intensities, respectively. In this experimental setup, excessive uptake manifests in an increase in these parameters compared with control cells (Figure 1, J and N and Supplemental Figure S1, A and P), as seen in the case of Rab5 overexpression, a known enhancer of endocytic activity (Bucci *et al.*, 1992; Atienza-Manuel *et al.*, 2021) that we used as a positive control (Figure 1, K and N and Supplemental Figure S1, B and P). Similarly, *snz* knockdown (Figure 1L and Supplemental Figure S1C) or *snz* knockout (Figure 1M and Supplemental Figure S1D) leads to a striking, statistically significant increase in the tracer-covered area (Figure 1N) and also to increased fluorescence intensities compared with the control cells (Supplemental Figure S1P), although this increase was not statistically significant in case of *snz* knockdown. Note that the enlarged endosomes are present in the subcortical region of these cells. We observed similar changes upon expression of GTP-locked Rab11,

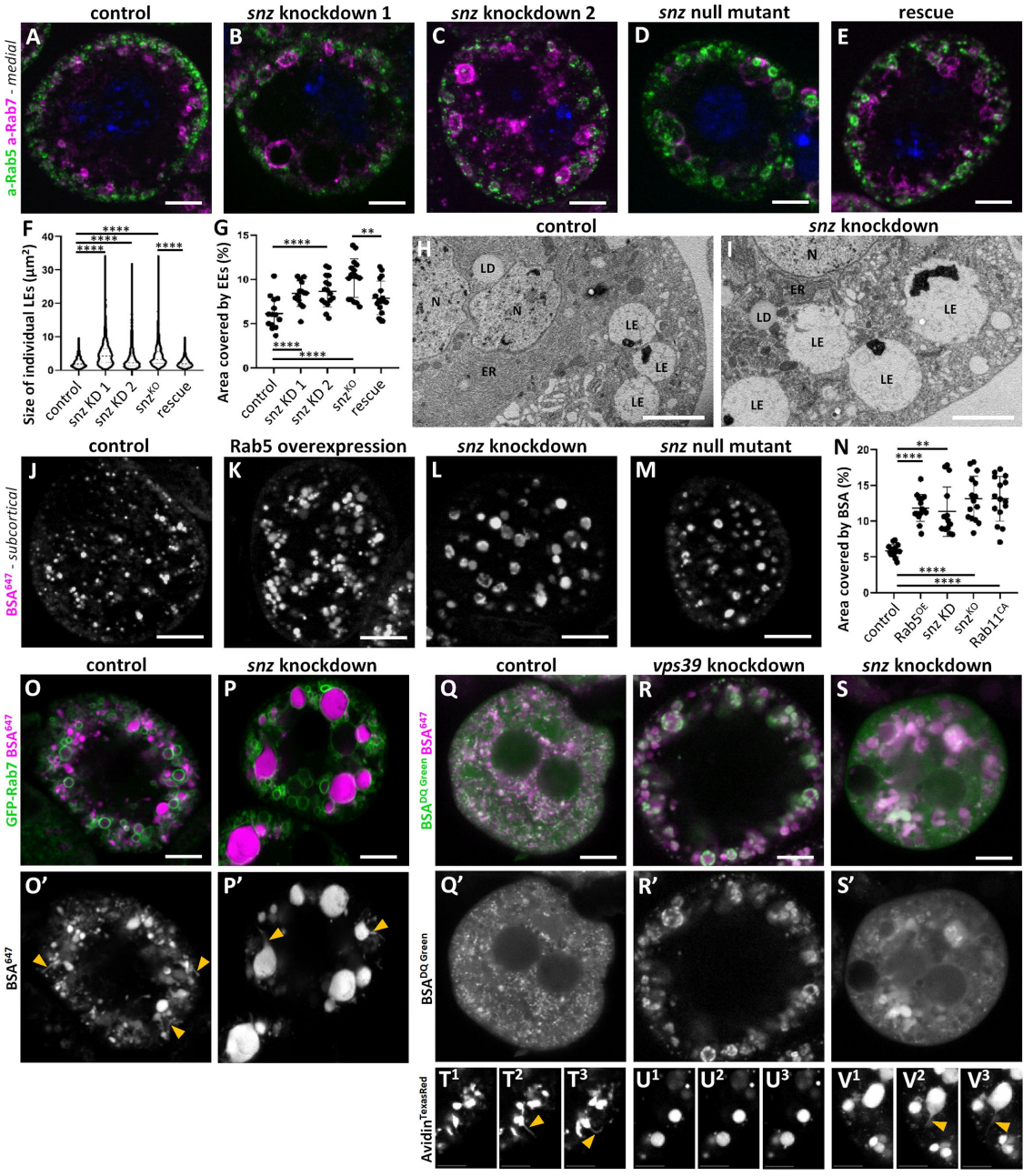

FIGURE 1: Loss of Snz enhances endocytic activity in nephrocytes. (A–E) Rab5 and Rab7 immunostaining of nephrocytes reveals the enlargement of early endosomes (EEs) and late endosomes (LEs), respectively, in *snz* knockdown (B and C) and knockout cells (D) compared with controls (A) and rescued mutants (E). (F and G) Quantification of data from panels A–E. (H and I) Ultrastructural analysis of control and *snz* knockdown nephrocytes. LEs, appearing as large, circle-shaped, electron-lucent vesicles with patches of a characteristic electron-dens material, are greatly enlarged upon loss of *snz*. (J–M) Pulse-chase labeling of nephrocytes after a 1-min pulse, followed by a 9-min chase using fluorescently labeled BSA as an endocytic tracer. Compared with controls (J), increased amount of tracer is detected in the subcortical region of Rab5 overexpressing (K), *snz* knockdown (L), and *snz* knockout (M) nephrocytes. (N) Quantification of the tracer-positive area from medial sections shown in panels S1A–E. (O and P) Pulse-chase labeling of GFP-Rab7-expressing nephrocytes after a 5-min pulse, followed by a 20-min chase using fluorescently labeled BSA as an endocytic tracer. (Q–S) Pulse-chase labeling of nephrocytes using $BSA^{DQ\ Green}$ and BSA^{647} as endocytic tracers. After a 5-min pulse, followed by a 1-h chase, the detected green signal represents dequenched, fluorescent products of $BSA^{DQ\ Green}$ degradation. Dequenching of DQ Green is observed only in patches within enlarged vesicles that accumulate BSA^{647} in *vps39* knockdown nephrocytes due to a block of endocytic progression (R), while the green signal appears both in vesicles and in the cytosol in control (Q) and *snz* knockdown (S) cells, indicating that endocytic degradation of the tracer is followed by its release to the cytosol. For quantification, see Supplemental Figure S1Q. (T–V) Frames from Supplemental movies V1–V3 show $Avidin^{TexasRed}$-positive endosomal compartments. Arrowheads point to tracer-positive tubules that are characteristic for actively digesting lysosomes. ER, endoplasmic reticulum; LD, lipid droplet; LE, late endosome; N, nucleus. Scale bars represent 5 µm in all panels. A *p* value of less than 0.05 was considered to be significant; * means $p < 0.05$; ** means $p < 0.01$; *** means $p < 0.001$, **** means $p < 0.0001$.

a key positive regulator of REs (Figure 1N and Supplemental Figure S1, E and P). These suggest increased endocytic activity in *snz* LOF nephrocytes.

To monitor later steps of endosomal maturation, live nephrocytes expressing the GFP-Rab7 reporter were allowed to take up BSA^{647} from the culture medium for 5 min (pulse) and were subjected to live imaging after 20 min (chase). In control cells (Figure 1O), the tracer appeared in the inner regions of the cells where it filled up spherical vesicles encircled by GFP-Rab7 and additional Rab7-negative compartments with irregular shape and with signs of tubulation (Figure 1O'). Such tubules are considered as the hallmarks of actively digesting lysosomes that constitute the so-called terminal lysosomal network in the perinuclear region of nephrocytes (Lund *et al.*, 2018). In the case of *snz* knockdown cells (Figure 1P), BSA^{647} accumulated in compartments demarcated by GFP-Rab7, showing that these enlarged LEs receive the incoming cargo. Tubulation of tracer-positive vesicles can also be frequently observed in these cells (Figure 1P') suggesting that actively digesting lysosomes are present in *snz* knockdown nephrocytes.

To test this more directly, we added BSA^{647} and $BSA^{DQ\ Green}$ to the medium of cultured nephrocytes for a 5-min pulse period, followed by 1-h chase, allowing the tracers to reach lysosomes. Fluorescence of $BSA^{DQ\ Green}$ is quenched in its intact form, while its degradation by proteases leads to the formation of highly fluorescent products. In control nephrocytes (Figure 1Q), fluorescence of $BSA^{DQ\ Green}$ can be detected in vesicles with variable sizes as well as in the cytosol indicating that degradation products are present in and also released from lysosomes. In contrast, inhibiting lysosomal delivery of the tracer by knocking down the gene encoding the key HOPS subunit Vps39 strongly decreases cytoplasmic green fluorescence (Figure 1R). In this case, the tracers are trapped in enlarged LEs that are located at the nephrocyte periphery due to the lack of HOPS-mediated fusion of LEs and lysosomes. Here, $BSA^{DQ\ Green}$ can be subjected to only partial degradation (indicated by patches of the green signal) without substantial release to the cytoplasm. This leads to a significantly higher vesicular versus cytoplasmic green fluorescence ratio in *vps39* knockdown cells compared with control nephrocytes (Supplemental Figure S1Q). In the case of *snz* knockdown cells (Figure 1S), the ratio of vesicular versus cytosolic fluorescence of $BSA^{DQ\ Green}$ does not differ significantly from the control (Supplemental Figure S1Q). Live imaging revealed the extensive formation of tracer-positive tubules with a highly dynamic behavior after a 30-min chase in control cells (Figure 1, T^1–T^3 and Supplemental movie V1). Such tubules are absent in *vps39* knockdown cells, indicating the lack of actively digesting lysosomes (Figure 1, U^1–U^3 and Supplemental movie V2). Importantly, dynamic tubulation of tracer-positive compartments is readily detected in *snz* knockdown cells, indicating efficient trafficking to digesting lysosomes (Figure $1V^1$–V^3 and Supplemental movie V3). To further assess lysosomal function, we performed Lysotracker Red and Lamp-GFP assays in nephrocytes and measured both the mean fluorescence intensities and the area of cells covered by these markers. Using the Lysotracker Red dye, acidic lysosomes can be readily detected in control (Supplemental Figure S1F) and *snz* knockdown (Supplemental Figure S1G) or null mutant cells (Supplemental Figure S1H), unlike in the case of the *vha16-1* V-ATPase subunit knockdown (Supplemental Figure S1I) where acidification of lysosomes is abrogated (Formica *et al.*, 2021) leading to a significantly decreased Lysotracker Red signal (Supplemental Figure S1J). To further confirm that functional lysosomes are present in *snz* LOF cells, we assessed lysosomal turnover of the Lamp-GFP reporter. The signal of its luminal GFP is quenched upon delivery to digesting lysosomes, while it remains fluorescent in the case of lysosomal degradation defects (Lund *et al.*, 2018; Milosavljevic *et al.*, 2022). Accordingly, control cells show low GFP fluorescence (Supplemental Figure S1K). In the case of *snz* knockdown (Supplemental Figure S1L) or null mutant (Supplemental Figure S1M) cells, the GFP signal is even mildly decreased compared with control cells. In contrast, the acidification-defective *vha16-1* knockdown cells contain large GFP-positive vesicles that most probably correspond to dysfunctional lysosomes (Supplemental Figure S1N), and GFPfluorescence is high in these cells (Figure S1O). Based on these results, we assume that endosomal flux, that is, the uptake and processing of cargo (including its transport to and degradation in lysosomes) is not impaired in *snz*-depleted cells.

Taken together, these results show that lysosomal degradation proceeds normally in nephrocytes with decreased *snz* function. The increased amount of endocytic cargo taken up by enhanced endocytic activity appears to slightly exceed the degradative capacity of *snz* LOF nephrocytes, leading to a partial congestion of the endosomal system that manifests in the expansion of the EE population and the presence of enlarged LEs over time during the 5 d of larval development.

Snz colocalizes with and binds to Rab11 in nephrocytes independently of ER-PM-LD contact sites

Next, we analyzed the localization of Snz in nephrocytes to understand its role in the endosomal system. We labeled various endomembrane compartments in nephrocytes expressing the GFP-tagged, full-length Snz reporter. Snz-GFP is peripherally distributed in these cells and forms a network composed of irregularly shaped, tubulovesicular structures with sizes ranging from a few hundred nm-s up to 2–3 µm-s (Figure 2, A–D, and Supplemental Figure S2). Surprisingly, and in contrast to the pronounced effect of *snz* loss on the morphology of Rab7-positive LEs, Snz-GFP does not colocalize with Rab7 (Figure 2E). In fact, the two signals occupy different regions of the cells with Snz-GFP being more peripheral than the layer of LEs (Supplemental Figure S2A). Rab5-positive EEs are close to Snz-GFP-positive structures in the cell periphery (Supplemental Figure S2B), and mild colocalization of the two signals can be detected (Figure 2E). Based on anti-Hrp staining, Snz-GFP–positive structures are positioned right beneath the PM and the two signals do not overlap (Figure 2E). Moreover, a mutually exclusive pattern of Snz-GFP and anti-Hrp can be recognized in the cortical zone of the cells (Figure 2A), indicating that Snz is excluded from the PM of nephrocytes. Thus, structures that are positive for Snz-GFP seem to be clustered in the nephrocyte periphery, more precisely in the interlacunar spaces created by the invaginations of the PM.

Snz was described in *Drosophila* fat cells as a member of membrane contact sites in triorganellar junctions formed by ER cisterns, the PM, and peripheral LDs (Ugrankar *et al.*, 2019). We wanted to know whether nephrocytes have similar contact sites and if such contacts exist, whether Snz is recruited to these in nephrocytes or not. To this end, we used the dMAPPER-Cherry reporter (Chang *et al.*, 2013) that marks ER-PM contacts and forms strongly fluorescent foci in the periphery of fat cells. Interestingly, dMAPPER-Cherry does not form discrete foci in nephrocytes; rather, it shows a bipartite distribution in the perinuclear and peripheral regions of the cells, reminiscent of the organization of ER cisterns (Figure 2B and Supplemental Figure S2C). Notably, no Snz-GFP colocalization can be observed with either dMAPPER-Cherry or the ER marker Cnx99A (Figure 2E). Based on our observations, unlike fat cells, nephrocytes do not seem to contain ER-PM contact sites that would recruit dMAPPER-Cherry and

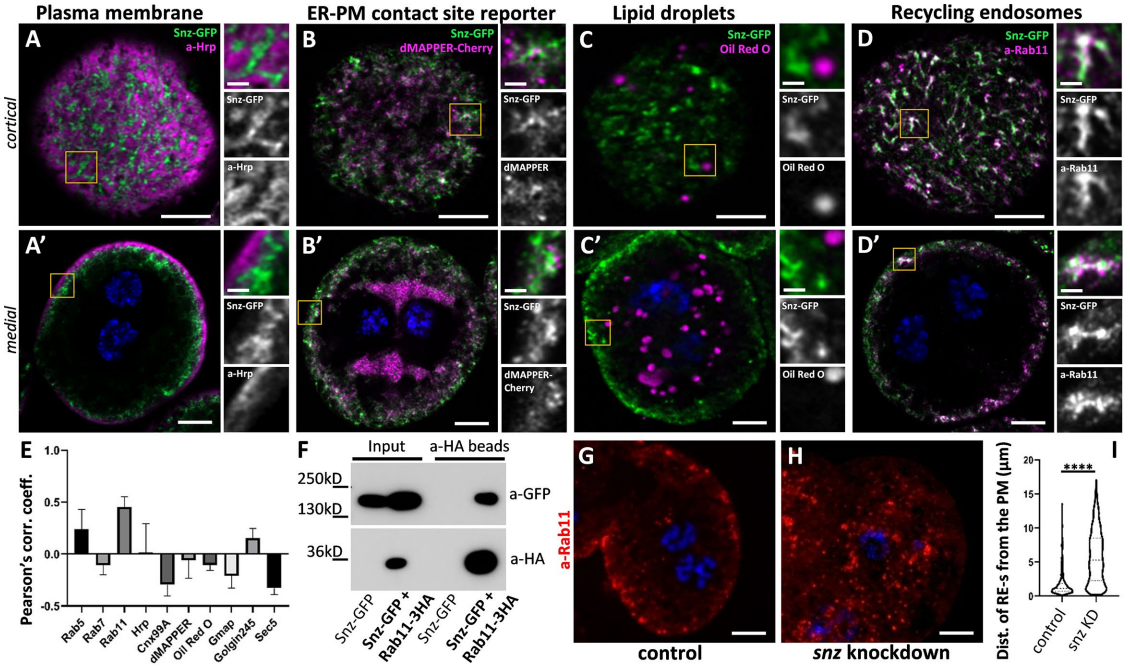

FIGURE 2: Snz colocalizes with and binds to Rab11 in nephrocytes. (A–D) Snz-GFP expressing nephrocytes stained for various organellar markers. Cortical (A–D) and medial (A′–D′) sections are shown in each case. No overlap is seen with the PM-marker anti-Hrp (A), the ER-PM contact site reporter dMAPPER-Cherry (B), and lipid droplets (LDs) labeled with Oil Red O (C). Snz-GFP shows extensive colocalization with Rab11-positive REs (D). Insets show the areas marked by yellow rectangles in higher magnification. (E) Quantification of data from A–D and Supplemental Figure S2A–S2F. (F) Coimmunoprecipitation from fly lysates shows the binding of Snz-GFP to Rab11-3xHA. (G and H) Rab11 immunostaining of control (G) and *snz* knockdown (H) nephrocytes. (I) Quantification of data from G and H. Scale bars represent 5 µm in the main panels and 1 µm in insets. ER, endoplasmic reticulum; PM, plasma membrane; RE, recycling endosome. A *p* value of less than 0.05 was considered to be significant; * means $p < 0.05$; ** means $p < 0.01$; *** means $p < 0.001$, **** means $p < 0.0001$.

therefore this reporter is distributed throughout the ER. We also wanted to test whether Snz is recruited to LDs in nephrocytes. LDs, while present in nephrocytes (Figure 2C), are mostly located in the inner regions of the cells and do not colocalize with Snz-GFP–positive structures (Figure 2E). These results indicate that in contrast to fat cells, nephrocytes do not contain ER-PM-LD contact sites that would recruit Snz.

In search for the identity of Snz-GFP-positive structures, we labeled further endomembrane compartments such as the *cis*- and *trans*-Golgi and the exocyst complex with anti-Gmap, anti-Golgin245, and anti-Sec5 antibodies, respectively (Supplemental Figure S2, D–F). No colocalizations with Snz-GFP can be detected in the case of the Gmap and Sec5 markers, and rare colocalization in the case of Golgin245 (Figure 2E). Ultimately, we found a striking colocalization of Snz-GFP with the Rab11-positive recycling compartment (Figure 2E) that also shows peripheral distribution in nephrocytes (Figure 2D). Moreover, physical interaction between full-length Snz-GFP and Rab11-3xHA proteins was evident in coimmunoprecipitation experiments using fly lysates (Figure 2F).

Given the colocalization and interaction of Snz and Rab11, we wanted to test the effect of *snz* LOF on the localization of Rab11-positive structures in nephrocytes. Compared with control cells (Figure 2G), endogenous Rab11-positive structures relocalize from the cell periphery to the inner regions and are scattered throughout the cytoplasm of *snz* knockdown nephrocytes (Figure 2H). The distance of Rab11 dots from the PM significantly increases in *snz* knockdown cells compared with controls (Figure 2I), indicating that proper distribution of REs depends on *snz* in nephrocytes.

Taken together, these results point to an ER-PM-LD contact site-independent function of Snz in nephrocytes at the Rab11-positive RE compartment.

Snz modulates Rab11 during the maintenance of diaphragm and lacunar channel integrity in nephrocytes

Next, we aimed to analyze the Rab11-related functional consequences of *snz* loss in nephrocytes. Components of the ND are in continuous turnover that requires intact EE and RE functions, which are controlled by Rab5 and Rab11, respectively (Wen *et al.*, 2020). Thus, changes in ND pattern potentially reflect on impaired endosomal trafficking in nephrocytes that can be a consequence of altered Rab5 or Rab11 functions. To this end, we immunolabeled Sticks and stones (Sns) and Polychaetoid (Pyd) proteins to visualize ND in heat-fixed samples. These diaphragm proteins reveal a strictly organized, fingerprint-like pattern—corresponding to the entrances of the lacunar channels—at the cortical region of control nephrocytes (Figure 3, A and A[1]) (Weavers *et al.*, 2009; Zhuang *et al.*, 2009), while in medial cross-sections, the Sns and Pyd signals appear as a line of tightly arranged ND units (Figure 3, A′ and A″ and Supplemental Figure S3A). In *snz* knockdown nephrocytes, such straight and parallel lines are rarely seen at the cortical region (Figure 3, B and B[1]), indicating that the architecture of lacunar channels is mildly affected. We detected the accumulation of Sns and Pyd in the inner regions of *snz* knockdown cells as well (Figure 3, B′ and B″ and Supplemental Figure S3B), suggesting that Snz is involved in the trafficking of ND proteins. Of note, the intracellular Sns and Pyd accumulation in *snz* knockdown cells can be rescued by abrogating exocyst function through the simultaneous knockdown of *sec5*

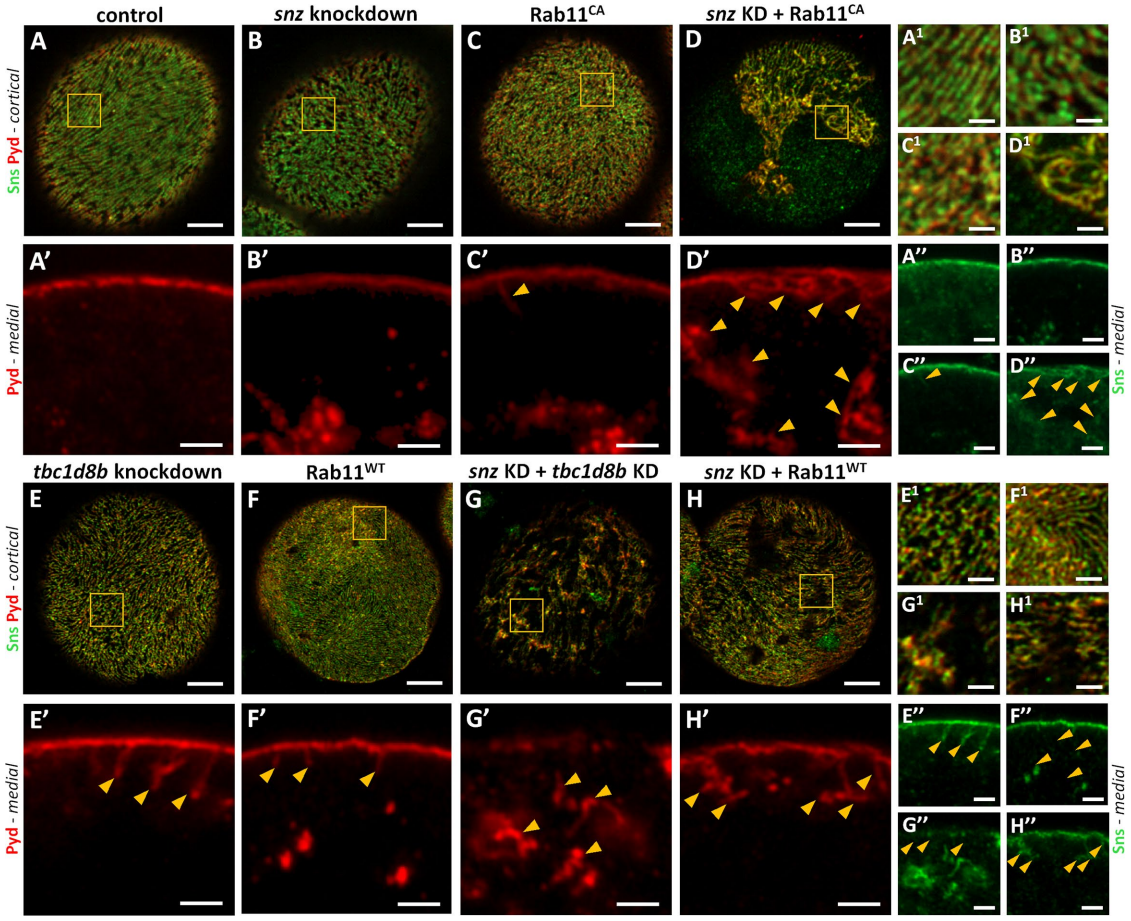

FIGURE 3: Snz modulates Rab11 activity for the proper maintenance of nephrocyte diaphragm (ND) integrity. ND patterns are visualized by Sns and Pyd immunostaining in heat-fixed nephrocytes. Cortical sections (A–H) show ND pattern at the cell surface and (A^1–H^1) show higher magnifications of the areas in yellow rectangles. Medial sections (A′–H′ for Pyd and A″–H″ for Sns) show cross-sectional views of ND units and deeper regions of nephrocytes. Arrowheads show ectopic NDs. Compared with the control (A), knockdown of *snz* (B) causes relatively mild alterations in the distribution of diaphragm components. This effect is similar to those seen upon expression of $Rab11^{CA}$ (C), knockdown of the Rab11 GAP *tbc1d8b* (E), or overexpression of $Rab11^{WT}$ (F). Massive rearrangements of the ND pattern are obvious when *snz* knockdown is combined with $Rab11^{CA}$ expression (D), *tbc1d8b* knockdown (G), or $Rab11^{WT}$ overexpression (H). Scale bars represent 5 µm in panels (A–H), 2 µm in panels (A′–H′) and (A″–H″), and 1 µm in panels (A^1–H^1).

(Supplemental Figure S3C), raising the possibility that decreasing the rate of exocytosis compensates for the loss of *snz*. Rab11 knockdown results in severe disorganization of the ND (Fu *et al.*, 2017; Wen *et al.*, 2020) observed in the cortical region of smaller than control nephrocytes (Supplemental Figure S3G) without accumulation of Sns and Pyd in the inner regions (Supplemental Figure S3, G′ and G″). Interestingly, in nephrocytes expressing the EYFP-tagged, GTP-locked and presumably constitutively active form of Rab11 (for simplicity, hereafter referred to as $Rab11^{CA}$), we observed similar ND rearrangements and intracellular Sns and Pyd accumulation as in the case of *snz* loss (Figure 3, C and C^1 and Supplemental Figure S3D). In line with the binding of Snz to Rab11 and opposite effects of their modulation (Rab11 gain-of-function looks similar to Snz LOF), the intracellular Sns and Pyd accumulation in $Rab11^{CA}$ expressing cells can be rescued by the coexpression of Snz-GFP (Supplemental Figure S3E).

Ectopic NDs are observed as Sns- and Pyd-positive intracellular protrusions in nephrocytes expressing $Rab11^{CA}$ (Figure 3, C′ and C″). Formation of ectopic NDs was described in recent studies (Kampf *et al.*, 2019; Atienza-Manuel *et al.*, 2021) and in the case of Rab11 overexpression, it was interpreted as a result of increased secretion. Importantly, we found a striking enhancement of this phenotype when we combined *snz* knockdown with $Rab11^{CA}$ expression. In this case, ectopic Sns and Pyd form ruffles at the cell surface and also demarcates a network that penetrates deeply into the inner regions of the cells (Figures 3, D′ and D″ and Supplemental Figure S3F). In the cortical view of these nephrocytes, severely disorganized ND sections alternate with PM regions without recognizable ND units (Figure 3, D and D^1).

To further corroborate the functional interaction of Snz with Rab11, we used additional tools to modulate Rab11 function in nephrocytes. First, we knocked down *tbc1d8b* (a known GTPase-activating protein [GAP] activator of Rab11 [Kampf *et al.*, 2019]) alone or in combination with *snz* RNAi. As expected, loss of *tbc1d8b* leads to the formation of ectopic diaphragms (Figure 3, E′ and E″) and it has only a minor effect on the cortical diaphragm pattern (Figure 3, E and E^1). This effect is indistinguishable from $Rab11^{CA}$ expression (Figure 3, C and C^1) or $Rab11^{WT}$ overexpression (Figure 3, F and F^1) and thus represents a Rab11 gain-of-function phenotype. When combined with *snz* RNAi, *tbc1d8b* knockdown leads to

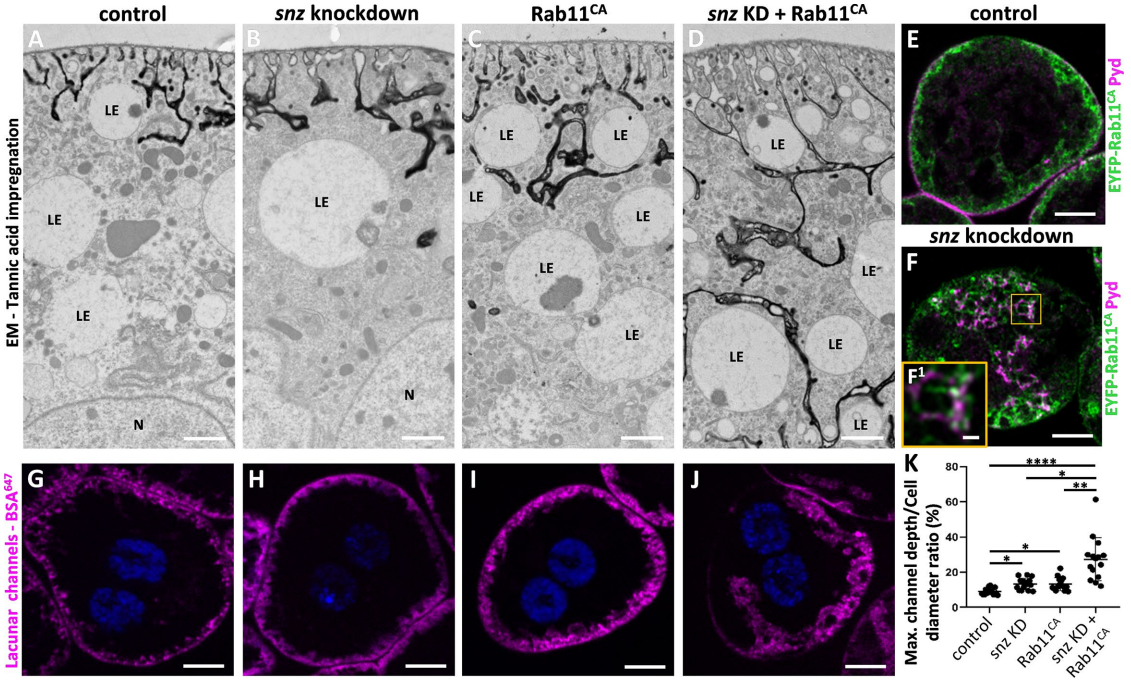

FIGURE 4: Snz and Rab11 control the depth of lacunar channels in nephrocytes. (A–D) Transmission electron microscopy (TEM) images of tannic acid impregnated cells, which highlights the lacunar system of nephrocytes (labeled by dark material). (E and F) Formaldehyde-fixed nephrocytes expressing EYFP-Rab11^{CA} immunostained for Pyd show that constitutively active Rab11 is present on the greatly expanded lacunar system in *snz* knockdown cells. (F^{1}) Higher magnification of the area in yellow rectangle. (G–J) Channel diffusion assay shows the depth of lacunar channels along the perimeter of whole cells. Note the presence of extremely elongated channels when *snz* knockdown is combined with Rab11^{CA} expression (D, F and J) compared with the control (A, E, and G), *snz* knockdown (B and H), or Rab11^{CA} expression (C and I) alone. (K) Quantification of data from panels G–J. Scale bars represent 1 µm in panels (A–D and F^{1}) and 5 µm in panels in panels (E–J). Medial sections are shown in (E–J). LE, late endosome, N, nucleus. A *p* value of less than 0.05 was considered to be significant; * means $p < 0.05$; ** means $p < 0.01$; *** means $p < 0.001$, **** means $p < 0.0001$.

much more severe disorganization of the diaphragm, which manifests in large-scale disruption in the cortical region (Figure 3, G and G^{1}) and formation of membrane ingressions containing ectopic diaphragm protein deposits in the medial region of nephrocytes (Figure 3, G′ and G″). This effect is highly similar to the effect of Rab11^{CA} expression (Figure 3C) or Rab11^{WT} overexpression combined with *snz* knockdown (Figure 3H). These results indicate that Rab11 gain-of-function perturbs diaphragm integrity and supports a role for Snz as a negative regulator of Rab11 in nephrocytes.

Ectopic ND deposits form in abnormally elongated lacunar channels of nephrocytes when either endocytosis is blocked or exocytosis is up-regulated (Kampf *et al.*, 2019; Atienza-Manuel *et al.*, 2021). Under these circumstances, excess membrane results in the elongation of lacunar channels toward the inner regions of the cells and PM proteins also populate these ingressions in the form of seemingly intracellular deposits. To visualize the lacunar network of nephrocytes, we carried out tannic acid impregnation, followed by EM imaging. Tannic acid does not penetrate through the PM, so it only labels those membranes and intermembrane spaces that are exposed to the extracellular milieu (Kosaka and Ikeda, 1983). In control nephrocytes (Figure 4A), lacunar channels form in the cortical region of the cells in an ~2–3 µm average depth. Somewhat deeper channels can be found in *snz* knockdown (Figure 4B) or Rab11^{CA} overexpressing cells (Figure 4C). Strikingly, tannic acid–positive, membrane-bound ingressions penetrate deep into nephrocytes when Rab11^{CA} is expressed together with *snz* RNAi (Figure 4D). In these cells, the PM invaginates into the inner regions of nephrocytes and lacunar channels form an extensive network of membrane ingressions that corresponds to the Pyd-labeled ectopic ND network in this genotype. Notably, intracellular diaphragm protein deposits can be recognized in EM images as electron dense ectopic diaphragms in the labyrinthine channels that penetrate to the deeper regions of nephrocytes (Supplemental Figure S3H). We also carried out formaldehyde fixation to enable the simultaneous visualization of the Pyd signal and Rab11^{CA}. In nephrocytes expressing only Rab11^{CA}, the protein localizes to the cortical region and it shows a pattern that most probably corresponds to the outline of the lacunar system (Figure 4E). It is likely that in this case, Rab11^{CA} cannot be released after Rab11-positive secretory vesicles fuse with the PM and it gets trapped in the membrane of the lacunar channels. Importantly, when Rab11^{CA} is expressed on a *snz* knockdown background, the resulting network-like Pyd signal overlaps with Rab11^{CA} (Figure 4, F and F^{1}), indicating that Pyd is found in ingressions formed by the PM. These results altogether demonstrate that knockdown of *snz* strongly enhances ectopic ND formation in elongated lacunar channels in Rab11-overexpressing nephrocytes, and that Snz overexpression counteracts Rab11^{CA}.

In a parallel set of experiments, we used the fluorescence-based channel diffusion assay (Milosavljevic *et al.*, 2022) where we applied BSA$^{Alexa-647}$ to fill up the labyrinthine channels (Figure 4, G–J), and we quantified the deepest channel depth to cell diameter ratio (Figure 4K). Compared with the control (Figure 4G), we found only a mild increase in *snz* knockdown (Figure 4H) or Rab11^{CA} expressing cells (Figure 4I). Strikingly, when we expressed Rab11^{CA} in a *snz* knockdown background (Figure 4J), it was found that tracer-filled

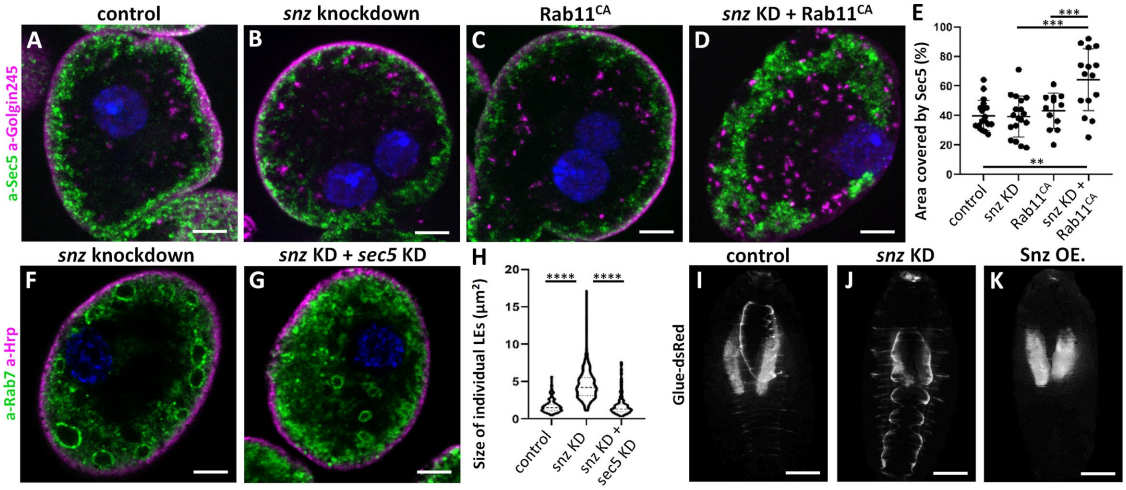

FIGURE 5: Snz is a negative regulator of exocytosis. (A–D) Sec5 and Golgin245 coimmunolabeling in nephrocytes visualizes the exocyst complex and the *trans*-Golgi network, respectively. Expression of Rab11^{CA} together with *snz* RNAi (D) results in massive expansion of the exocyst network and intracellular redistribution of Golgin245 compared with control (A) or either genetic manipulation alone (B and C). (E) Quantification of data from A–D. (F and G) Rab7 and Hrp staining of nephrocytes to label late endosomes (LEs) and the plasma membrane (PM), respectively. Enlarged endosomes are seen in *snz* RNAi cells (F, compare with the Rab7 structures seen in control cells in Figure 1A). Cosilencing of the exocyst component sec5 restores LE size to normal (although not their proper distribution, G) in *snz* knockdown cells. (H) Quantification of data from G, H, and control cells (not shown). (I–K) Prepupae expressing the Glue-dsRed reporter in salivary glands (SGs). Normally, only a subset of glue protein is secreted from SGs and released to the surface of the animals, while residual glue can be observed in SGs inside the pupal case (I). Overexpression of *snz* increases the amount of released glue (J), while its loss blocks glue release (K). Scale bars represent 5 µm in panels A–D, F–G, and 1 mm in panels I–K. A p value of less than 0.05 was considered to be significant; * means $p < 0.05$; ** means $p < 0.01$; *** means $p < 0.001$, **** means $p < 0.0001$.

channels penetrate much deeper into the cells in an asymmetric manner in most of the cases. Thus, a large amount of excess PM is generated and forms membrane ingressions in Rab11^{CA} expressing cells with decreased *snz* function.

We thus conclude that *snz* is required for maintaining ND and lacunar channel integrity, most probably through restricting Rab11-mediated recycling and exocytosis toward the PM.

Snz inhibits exocytosis

As endocytic degradation is not compromised and endocytic activity seems enhanced in *snz* knockdown cells, we hypothesized that loss of *snz* contributes to the formation of membrane ingressions through the up-regulation of exocytosis in nephrocytes. To investigate this, we examined the status of the secretory system by colabeling Golgin245 and Sec5 in nephrocytes as markers of the *trans*-Golgi network and the exocyst complex, respectively. In control cells, Golgin245-positive structures are present in the nephrocyte periphery, and they can also be found in small patches in the deeper regions of the cells (Figure 5A). Sec5 is distributed along the cell periphery in the form of small dots, which most probably represent exocyst complexes assembled on the surface of secretory vesicles prior to fusion and/or at docking sites where these vesicles are tethered to the PM. Importantly, knockdown of *snz* (Figure 5B) or expression of Rab11^{CA} (Figure 5C) alone does not lead to such large-scale alterations of Sec5 or Golgin245. Strikingly, in *snz* knockdown nephrocytes expressing Rab11^{CA} (Figure 5D), the Sec5-positive area is greatly increased compared with the other genotypes (Figure 5E). This can indicate the increased number of secretory vesicles that are distributed along membrane ingressions formed by the network of elongated lacunar channels. Interestingly, the distribution of Golgin245-positive structures is also altered in these cells. The peripheral Golgin245 signal is decreased or completely missing in most cells, while the number of patches in the deeper regions is markedly increased compared with the control. We interpret these results as the expansion and reorganization of the *trans*-Golgi network in *snz* knockdown nephrocytes that also express Rab11^{CA}. This indicates the synergistic effect of Snz loss and Rab11 gain in the secretory system of nephrocytes.

Next, we combined *snz* knockdown with *sec5* knockdown to investigate the role of exocytosis in the formation of *snz* LOF phenotypes. As the enlargement of LEs is a very robust response of nephrocytes to *snz* loss, we compared LE size in *snz* knockdown cells with *snz-sec5* double knockdown cells in an epistasis analysis. In contrast to the enlarged LEs of *snz* knockdown nephrocytes (Figure 5F), LE size was restored to normal in *snz-sec5* double knockdown cells (Figure 5, G and H). Thus, exocytic transport is required for the formation of enlarged LEs in *snz* knockdown cells.

To assess the role of *snz* in the regulation of exocytosis in another tissue, we monitored the release of secretory glue from *snz* knockdown and *snz* overexpressing salivary glands (SGs) at the onset of metamorphosis. Knockdown or overexpression of *snz* was driven by the fkh-Gal4 driver in SGs expressing a Glue-dsRed reporter (Costantino *et al.*, 2008; Csizmadia *et al.*, 2018). Glue is synthesized in and secreted from SGs of wandering larvae, and it mediates the strong attachment of the (pre)pupa to a solid surface during puparium formation. In the case of control animals (Figure 5I), traces of glue released from SGs can be observed beneath the prepupae facing the surface of the culture vial. Importantly, a significant amount of glue remains in SGs that can be seen inside the pupal case. In age-matched animals with *snz* knockdown in SGs (Figure 5J), the released glue covers a much larger surface under the prepupae, and SGs containing residual glue appear fainter than the control. This indicates increased glue release from SGs upon *snz* knockdown. Finally, we detected intense remaining dsRed fluorescence in

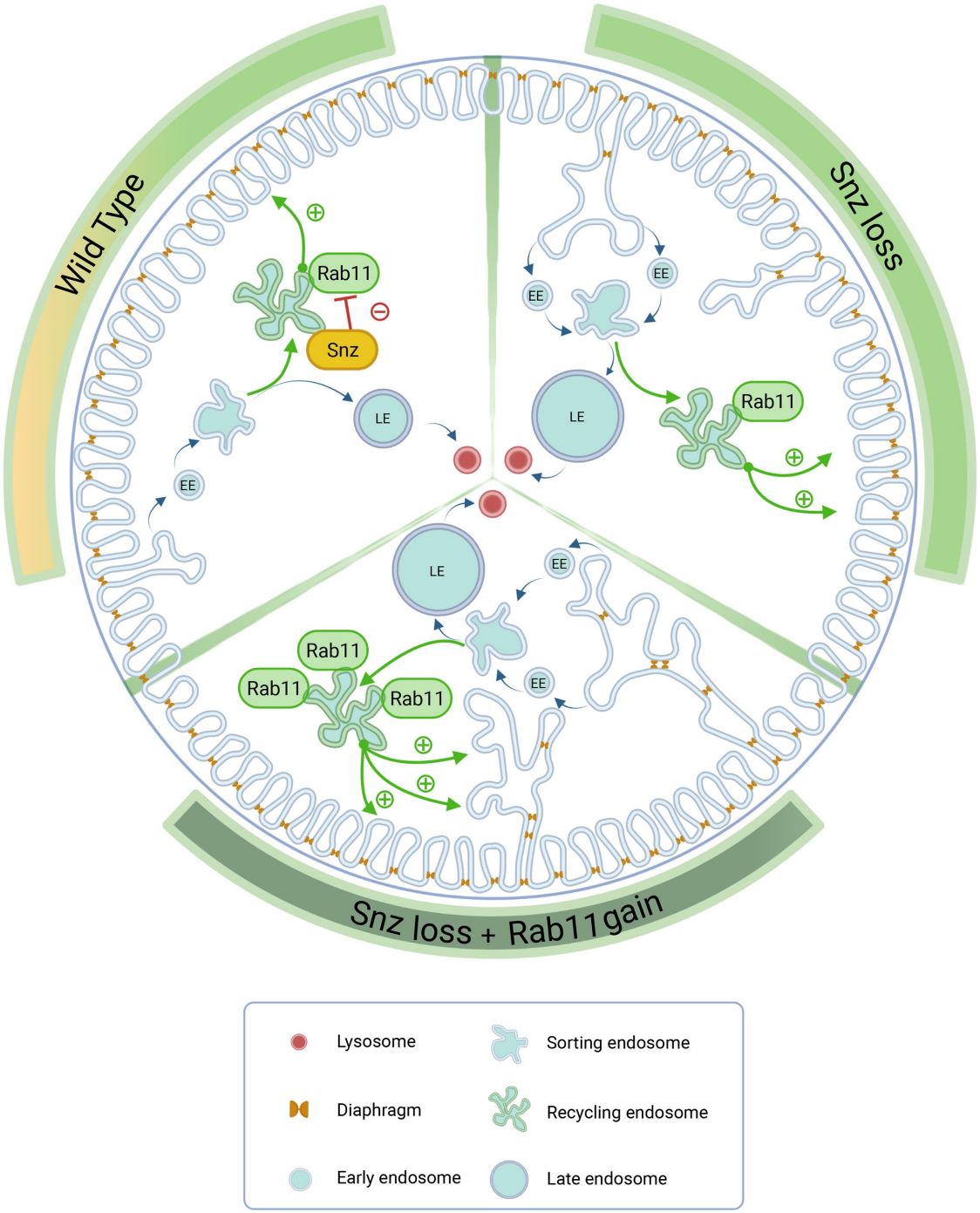

FIGURE 6: Snz is a negative regulator of Rab11-mediated recycling in *Drosophila* nephrocytes. Schematic shows that lacunar channel and diaphragm integrity are maintained by the balance of endocytic and exocytic trafficking in wild-type nephrocytes. Loss of Snz alone or combined with Rab11 gain-of-function leads to imbalances in membrane trafficking and prominent functional and morphological changes in the endosomal system. See the main text for further details. EE, early endosome; LE, late endosome. Created with BioRender.com.

SGs that overexpress *snz*, and at the same time no traces of glue are seen on the surface of prepupae, indicating glue release failure (Figure 5K). These observations indicate that Snz also regulates secretion in SGs, which further supports our findings in nephrocytes.

DISCUSSION

Based on our results described here, we favor a model in which the main role of Snz is the negative regulation of Rab11-mediated recycling in *Drosophila* nephrocytes (Figure 6), supported not only by its colocalization with and binding to Rab11 but also by the mutant/overexpression phenotypes and extensive genetic interaction data. We propose that decreased *snz* function enhances membrane flow from REs toward the PM. This would lead to the formation of membrane ingressions; however, no prominent elongation of lacunar channels can be observed in *snz* LOF nephrocytes. We assume that in this case, increased endocytosis compensates and it is sufficient to

counterbalance the excess amount of membrane that arrives from REs to the PM. This increased rate of endocytosis leads to a slight overload of the endosomal system, culminating over time (i.e., during the 5 d of larval development) in the striking expansion of the EE and LE endosomal populations in *snz* LOF nephrocytes. This role of exocytosis in the development of enlarged LEs is strongly supported by our finding that depletion of exocyst restores LE size and eliminates intracellular Sns and Pyd accumulation in *snz* knockdown nephrocytes. Similar to the effect of *snz* knockdown, Rab11 gain-of-function (via overexpressing the wild-type or GTP-locked form of Rab11 or knocking down *tbc1d8b* encoding a Rab11 GAP) does not lead to the formation of deep membrane ingressions on its own either, while Sns and Pyd again form intracellular deposits in $Rab11^{CA}$ expressing cells, similarly to *snz* knockdown. Notably, this phenotype can be rescued by the overexpression of Snz, indicating that Snz counteracts Rab11. Ectopic diaphragms are also frequently observed in $Rab11^{CA}$ expressing nephrocytes as the result of increased exocytosis (Kampf *et al.*, 2019). Importantly, expression of $Rab11^{CA}$ on a *snz* LOF background leads to partial breakdown of the nephrocyte surface diaphragm network and to the formation of deep membrane ingressions. We assume that in this case, excess membrane derived from REs is channeled toward the PM via massive exocytosis that far exceeds the capacity of compensatory endocytosis and leads to the uncontrolled elongation of labyrinthine channels. Similarly, rearrangements in the secretory system involving the *trans*-Golgi network and exocyst-positive vesicles are also apparent only in the case of simultaneous $Rab11^{CA}$ expression and *snz* knockdown. Snazarus was identified as a potential binding partner of Rab11 in a comprehensive interactome study of Rab small GTPases (Gillingham *et al.*, 2014), which we have now confirmed in our study. Together with our genetic interaction data, the binding of Snz to Rab11 raises the possibility that Snz itself restricts Rab11 activity.

Although the exact biochemical mechanism is yet to be confirmed, we assume that decreased *snz* function leads to the disinhibition of a molecular step in the recycling route that promotes membrane flow from REs toward the PM. Snz functionally interacts with the fatty acyl desaturase Desat1 in *Drosophila* fat tissue as part of ER-PM-LD contacts (Ugrankar *et al.*, 2019) and the contact site–dependent role of human SNX14 in lipid metabolism is also known (Datta *et al.*, 2019, 2020). Importantly, a recent study using AlphaFold2-based prediction reported that the PXA and PXC domains of Snx-TM proteins interact with each other to form a hydrophobic cavity with a presumable function of lipid binding and/or transfer (Paul *et al.*, 2022). These findings indicate the conserved role of Snx-TM proteins in lipid metabolism and transfer as parts of membrane contact sites. Thus, lipid transfer regulated by Snz might be also involved in its function. In line with this, ethanolamine addition rescues the autophagic defect caused by loss of Snz in *Drosophila* fat cells (Lauzier *et al.*, 2022). Nephrocytes must also depend on the trafficking of lipids as their endomembrane system undergoes continuous and intensive remodeling. In these cells, maintaining the balance of exocytosis and endocytosis is key to preserve the steady-state amount of not only proteins at the PM but also lipids/membrane. We think that Snz is a key player in regulating this kind of balance, and we cannot exclude the possibility that altered lipid composition also affects Rab11-dependent recycling events in nephrocytes in addition to the binding of Snz to Rab11.

The Rab11 small GTPase is a master regulator of cell surface protein composition in many cell types as it acts at the intersection of vesicular trafficking events directed toward the PM (Welz *et al.*, 2014). Accordingly, Rab11 is present on REs, post-Golgi vesicles, and also at the *trans*-Golgi network. Regulated by its activator guanine nucleotide exchange factor and deactivator GAP partners, Rab11 interacts with a variety of effector proteins including different motor protein complexes and the exocyst complex (Welz *et al.*, 2014). Through these interactions, Rab11 is involved in a variety of fundamental cellular processes such as receptor and adhesion protein recycling, cytokinesis, oogenesis, and so forth. *Drosophila* Rab11 is extensively investigated, and its function is described in glue granule maturation in the SG, rhodopsin recycling in photoreceptor cells, and also in diaphragm maintenance in nephrocytes (Satoh *et al.*, 2005; Wen *et al.*, 2020; Neuman *et al.*, 2021).

The involvement of Snx proteins in Rab11-mediated recycling has not been described previously, although the role of many sorting nexins in various vesicular trafficking processes is well established. The presence of the PI(3)P-binding PX domain in sorting nexins predestines these proteins to be involved primarily in endosome-associated sorting. Indeed, as parts of different sorting complexes such as the retromer, retriever, and recycler, Snx proteins contribute to the recycling of a multitude of endosomal transmembrane proteins from EEs or LEs toward various locations of the endosomal system (Chen *et al.*, 2019; Zhou *et al.*, 2022). Interestingly, both Snazarus and human SNX25 contain a noncanonical PX-domain, and alterations in their phospholipid-binding surfaces confer a broad specificity toward di- or triphosphorylated PI-derivatives. PI(4,5)P2 is the most abundant PI-derivative in the PM, and in *Drosophila* fat cells, Snazarus interacts with the PM through its noncanonical PX domain. As it has been recently shown, Snazarus has a dual role in *Drosophila* fat cells as it is involved in lipid metabolism and also in autophagy, which might also involve its binding to PI(3)P that is typically found in forming and mature autophagosomes. Thus, the role of Snz in both vesicular and nonvesicular trafficking within the same tissue is already known in *Drosophila* fat cells. Another interesting feature of Snx-TM proteins is the presence of an RGS (short for regulators of G protein signaling) domain, and it is tempting to speculate that Snz might directly regulate Rab11 in nephrocytes through this domain. This unique RGS domain is known to function as a GAP on trimeric G protein α subunits (Amatya *et al.*, 2021). It will be interesting to test in future studies whether the RGS domain of Snz/SNX25 might be able to bind to Rab11 and thus directly inactivate this small GTPase, although RGS domain binding to a small monomeric GTPase is unprecedented and so it seems unlikely.

Although the physiological function of SNX25, the human orthologue of Snz, is currently unknown, its role in vesicular trafficking was reported. SNX25 interacts with TGF-β receptors and enhances receptor degradation via the clathrin-dependent endocytosis and endosome/lysosome degradation pathway (Hao *et al.*, 2011). Human SNX25 is also involved in regulating autophagic flux via VAMP8 trafficking (Lauzier *et al.*, 2022). In recent studies, SNX25 has been associated with diseases such as temporal lobe epilepsy (Du *et al.*, 2013), colorectal cancer (Feng *et al.*, 2022), psoriasis (Vecellio *et al.*, 2021), and chronic kidney disease (CKD) (Kim *et al.*, 2021). In the latter case, SNX25 mutation is associated with higher activity of indoleamine 2,3-dioxygenase, a proposed CKD marker, and decreased glomerular filtration rate. Given the role of Snz in *Drosophila* nephrocytes, involvement of SNX25 in CKD is particularly interesting, although the effect of SNX25 mutations on human podocyte function has not been studied.

Importantly, our results point to a novel, RE-specific function of Snz that differs from its role in ER-PM-LD contact sites. In fat cells, the presence of such contacts is highly advantageous as they enable efficient response to altered nutritional conditions through the rapid mobilization of fatty acids. Although nephrocytes also contain LDs,

these cells are not specialized for lipid storage and mobilization; hence, the absence of ER-PM-LD contacts with fat cell-like functions is quite reasonable. It is obvious that Snz-GFP does not overlap with, and it is not even in the vicinity of, LDs in nephrocytes. LDs are found in the inner regions of these cells, while Snz-GFP localizes to Rab11-positive REs at the cell periphery. Here, an intricate network of lacunar channels is formed by the invaginations of the PM, which is dynamic with continuous vesicular fusion and fission events. The existence of membrane contact sites here, which could enable non-vesicular membrane transport, is also possible. The peripheral pool of the ER is also present here in the form of fine cisterns, raising the possibility that fat cell-like ER-PM contact sites might form in the periphery of nephrocytes. Although the dMAPPER-Cherry ER-PM contact site reporter does not show intensively fluorescent foci here, we cannot exclude the existence of such contacts based on our results. Accordingly, in some cases we saw partial overlap of Snz-GFP with dMAPPER-Cherry (Figure 2B). Based on this observation, one can imagine a scenario in which Snz acts as part of ER-PM contacts in nephrocytes that involves REs instead of LDs as a third organelle. The striking relocalization of REs in *snz* LOF cells may reflect on the role of Snz in stabilizing such contact sites and anchoring REs to the tips of PM channels. However, if ER-PM contacts indeed form in the nephrocyte periphery, one would expect a higher degree of colocalization of Snz with anti-Hrp and anti-Cnx99A that we used as PM and ER markers, respectively. A possible caveat is that although anti-Hrp is widely accepted to stain nephrocyte PM (Paschinger *et al.*, 2009; Atienza-Manuel *et al.*, 2021), deeper regions of lacunar channels do not seem to be labeled by this antibody. In the case of the ER, a fine network of peripheral ER cisterns with faint anti-Cnx99A signal is visible (Supplemental Figure S2C), and these ER cisterns occasionally overlap with Snz-GFP. Thus, there is a possibility that ER-PM-RE contact sites form in nephrocytes. These contacts could be involved in nonvesicular membrane transport processes between these organelles, which could also contribute to the intensive membrane remodeling events at the nephrocyte periphery. Such organelle contacts could also tether REs to peripheral ER and to lacunar PM channels to facilitate vesicular trafficking. This model is supported by the striking redistribution of Rab11 vesicles toward the cell interior in *snz* LOF nephrocytes.

Finally, the similar nephrocyte defects arising from Snz loss and Rab11 gain-of-function (seen not only upon expression of GTP-locked mutant Rab11 but also in case of wild-type Rab11 overexpression and knockdown of *tbc1d8b* encoding a Rab11 GAP, which inhibits Rab11 by stimulating its GTP hydrolysis), the strongly synergistic effect of Snz loss with Rab11 gain, and that Snz overexpression antagonizes the effects of Rab11 gain-of-function and restores a wild-type nephrocyte phenotype collectively argue that these two proteins function together at REs. We would like to emphasize that all the alterations arising upon modulation of Snz levels that we report here can be explained completely by its inhibitory effect on Rab11 activity, both in case of endosomal trafficking and exocytosis. Increased endocytic flux and recycling due to higher Rab11 activity in the absence of Snz likely result in increased exocytosis, which seems to be restored to normal levels in nephrocytes via attenuation of exocyst function, in line with our model as the exocyst is a known Rab11 effector. The recently described Rab11-dependent endocytic contribution to secretory granule maturation that promotes glue release in SGs (Ma *et al.*, 2020) is also perfectly in line with the phenotypes that we see upon modulation of Snz levels, because its SG-specific overexpression inhibits glue release (possibly via decreasing Rab11 activity) whereas its loss enhances secretion (probably because of increased endocytic input to secretory glue granules). In conclusion, we demonstrate here a new role for the sorting nexin 25 homologue Snazarus: its binding to and functional inhibition of Rab11 at REs.

MATERIALS AND METHODS

Request a protocol through *Bio-protocol*.

Drosophila strains and genetics

Flies were raised on standard yeast/cornmeal/agar media at room temperature. Fly stocks used in this study were obtained from the Bloomington Drosophila Stock Center (BDSC), from the Vienna Drosophila Resource Center (VDRC), or from FlyORF and were the following: mCherry RNAi (control) [BDSC 35785], snz RNAi 1. [BDSC 39036], snz RNAi 2. [VDRC 105671], vps39 RNAi [VDRC 40425], vha16-1 RNAi [VDRC 49291], sec5 RNAi [BDSC 27526], Rab11 RNAi [BDSC 27730], tbc1d8b RNAi [BDSC 32929], UAS-GFP-Rab5 [BDSC BL43336], UAS-EYFP-Rab11^{Q70L} (Rab11^{CA}) [BDSC 9791], and UAS-EYFP-Rab11-3xHA [FlyORF F001035]. The prospero-Gal4 driver was obtained from Bechtel *et al.* (2013) and the Glue-dsRed; fkh-Gal4 stock was obtained from Costantino *et al.* (2008). The snz^{KO} line, the UAS-dMAPPER-Cherry, and UAS-Snz-GFP reporters were described in Ugrankar *et al.* (2019). Additional genotypes were the following: hs-Flp; UAS-Dcr2; Actin>CD2>Gal4 UAS-Rab7-GFP and hs-Flp; UAS-Dcr2; and Actin>CD2>Gal4 UAS-Lamp1-GFP (Lőrincz *et al.*, 2016). Standard genetic crosses were used to recombine the UAS-Snz-GFP or the UAS-EYFP-Rab11^{Q70L} reporters to the prospero-Gal4-containing or tub-Gal4 containing chromosome. In the case of the rescue experiments, we established a stable stock with the following genotype: snz^{KO}; +; prospero-Gal4; and UAS-Snz-GFP/TM6Tb.

Immunolabeling and Lysotracker Red staining

Immunostaining of formaldehyde-fixed nephrocytes was performed as described in Lőrincz *et al.* (2016). Briefly, wandering larvae were dissected in PBS and fixed with 4% formaldehyde. Samples were extensively washed with PBS and then incubated in PBTx (0.1% Triton X-100 in PBS) for 30 min. After blocking with 5% FCS-containing PBTx, samples were incubated overnight at 4°C in the blocking solution completed with primary antibodies. Samples were then rinsed, extensively washed, and then were incubated in the blocking solution containing the appropriate secondary antibodies for 2 h at room temperature (RT). After rinsing and washing, nuclei were stained with 2-(4-amidinophenyl)-1H-indole-6-carboxamidine (DAPI). For Oil Red O staining, at this point we added freshly prepared, filtered 2:3 mixture of distilled water and 0.1% Oil Red O (Sigma-Aldrich #O0625) solution (in isopropanol) to the samples, followed by extensive washing with PBS. Samples were mounted in Vectashield. Heat fixation of nephrocytes was performed as described in Hochapfel *et al.* (2017). Briefly, stage L3 larvae were dissected in PBS and then the gut segments were put in boiling 0.03% PBTx and immediately microwaved for 20 s in water bath. After that, they were washed in TWEEN 20-PBS and then blocked in BSA solution for an hour. Samples were incubated with a-Sns and a-Pyd primary antibodies overnight at 4°C. After extensive washing, appropriate secondary antibodies were added to the samples for 2 h at RT and then washed again and mounted. The following primary antibodies were used: polyclonal rabbit a-Rab11 (1:400; Tanaka and Nakamura, 2008), polyclonal chicken a-Sns (1:1000; Hochapfel *et al.*, 2017), monoclonal mouse a-Sec5 (1:35; Murthy *et al.*, 2003), polyclonal rabbit a-Rab5 (1:100; Abcam #31261), monoclonal mouse a-Rab7 (1:10; DSHB), monoclonal mouse a-Cnx99A (1:200; DSHB), monoclonal mouse a-Pyd (1:400; DSHB), polyclonal goat a-Gmap (1:2000; DSHB), polyclonal goat

a-Golgin245 (1:2000; DSHB), polyclonal chicken a-GFP (1:400; 2BScientific #AGFP-NM), and polyclonal Alexa Fluor 647 goat a-Hrp (1:800, Jackson Immunoresearch #2338967). Secondary antibodies were FITC donkey antichicken, Alexa Fluor 488 goat antirabbit, Alexa Fluor 488 goat antichicken, Alexa Fluor 568 goat antirabbit, Alexa Fluor 568 goat antimouse, Alexa Fluor 568 donkey antigoat, Alexa Fluor 568 donkey antimouse, and Alexa Fluor 647 rabbit antimouse (all 1:800; all Invitrogen—ThermoFisher Scientific). For LysoTracker Red staining, larval garland nephrocytes were incubated in medium containing LysoTracker Red (1:1000; ThermoFisher Scientific # L7528) for 5 min at RT. Samples were rinsed three times, stained with DAPI, and imaged immediately.

Tracer uptake and channel diffusion assay

Nephrocytes of wandering-stage larvae were dissected in freshly prepared Shields and Sang M3 insect medium (Sigma-Aldrich #S8398). Cells were incubated in M3 medium completed with $BSA^{DQ\ Green}$ (Thermo Scientific #D12050), $BSA^{Alexa\text{-}647}$ (Thermo Scientific #A34785), or $Avidin^{TexasRed}$ (Thermo Scientific #A820) at 80 µg/ml concentration for 5 min (pulse) and then washed out. Cells containing internalized tracers were then imaged after 20-min or 1-h chase intervals. In the case of tracer uptake experiments with short incubation times, nephrocytes were allowed to take up $BSA^{Alexa\text{-}647}$ for 1 min, and after a 9-min chase they were fixed in 4% formaldehyde, washed extensively with PBS, and then DAPI staining was applied. Channel diffusion assay was carried out as described recently (Milosavljevic *et al.*, 2022).

Imaging, quantification, and statistical analysis

All stainings have been carried out at least twice (technical replicate), with similar results. Images were taken with a Zeiss Axio Imager.M2 fluorescent microscope equipped with ApoTome.2 or a ZEISS LSM 800 confocal microscope with Airyscan using 1.4 NA 63 × (Oil) Plan-Apochromat objectives in both cases. Images were captured and their brightness and contrast were adjusted uniformly with the Zeiss ZEN Pro software to preserve all potentially important information. Microscope and imaging settings were identical for experiments of the same kind. In general, three to five nephrocytes per animal were selected for quantification. Only cells that were optically sectioned in the middle part were included in the analysis to avoid distortion of data or undersampling. In addition, in some of our experiments we imaged cortical and subcortical sections for demonstration purposes as it is indicated in the figures and figure legends. Images were analyzed with the Zeiss ZEN Pro and ImageJ softwares. The levels of noise- and background staining were reduced by applying a uniform threshold for the same type of experiments using ImageJ. We determined the percentage of cell area covered by the corresponding cytoplasmic markers after subtracting the nuclear area (based on DAPI counterstaining) from the measured whole cell area. To measure LE size, we selected the Rab7-positive rings one by one—endosome sizes are profile areas measured in square micron. For colocalization analyses, we measured Pearson's correlation coefficient of red and green channels using the coloc2 plugin of ImageJ (1 = perfect colocalization, 0 = no/incidental colocalization, and −1 = mutually exclusive localization). In the case of Rab11-positive structures, their distances from the PM were measured one by one. Lacunar channel depth was quantified by measuring the diameter of the approximately sphere-shaped nephrocytes comparing it with the maximum channel depth measured along a line perpendicular to the cell surface. The Zeiss Zen software was used to measure cytoplasmic versus vesicular $BSA^{DQ\ Green}$ intensity. First, whole cell signal intensities were quantified and then thresholding was applied to aid the identification of vesicular structures showing higher signal intensity compared with the cytosol. We calculated the cytosolic signal intensity by measuring sum signal intensities in vesicles and subtracting them from the whole cell signal intensities. Statistical analysis was performed with GraphPad Prism using the tests indicated in Supplemental Table S1. A p value of <0.05 was considered to be significant; * means $p < 0.05$; ** means $p < 0.01$; *** means $p < 0.001$, and **** means $p < 0.0001$.

EM analysis

Nephrocytes were dissected in ice-cold PBS and then were fixed in 3.2% PFA, 0.5% glutaraldehyde, 1% sucrose, and 0.028% $CaCl_2$ in 0.1 N sodium cacodylate, pH 7.4, overnight at 4°C. Samples were then postfixed in 0.5% osmium tetroxide for 1 h, washed with distilled water (2*5 min at RT), and then treated with half-saturated aqueous uranyl acetate for 30 min at RT. Samples were then dehydrated in a graded series of ethanol and embedded in Spurr resin (Merck) according to the manufacturer's recommendations. A total of 70-nm sections were stained with Reynold's lead citrate and viewed on a JEM-1011 transmission electron microscope (Jeol) equipped with a Morada digital camera (Olympus) using iTEM software (Olympus). Tannic acid impregnation was performed as described (Kosaka and Ikeda, 1983). Briefly, samples were processed for electron microscopy as mentioned previously but after the osmification step samples were treated with 1% tannic acid (Merck) in 0.1-M cacodylate buffer (pH 7.4) for 30 min at RT and uranyl acetate treatment was omitted.

Coimmunoprecipitation

Approximately 200-mg adult flies of either snz^{KO}; tub-Gal4, UAS-Snz-GFP/+, or snz^{KO}; tub-Gal4, UAS-Snz-GFP/UAS-Rab11-3xHA genotypes were dounce homogenized in 2 ml of LBW buffer (lysis, binding, and wash: 25-mM Tris-HCl pH 7.5, 5-mM $MgCl_2$, 20-mM KCl, 100-mM NaCl, 0.1x PBS, 10% glycerol, and 0.2% Triton X-100). Extracts were clarified by repeated centrifugation, taking care to leave as much of the upper fatty layer of the lysate behind as possible at each step. Extracts were further clarified by letting them pass through 300-µl Sephadex-G100 packed into disposable plastic columns by gravity flow. Extracts (750 µl) were incubated with 25-µl anti-HA magnetic beads (Pierce 88837) for 4 h, washed extensively, and eluted by using nonreducing SDS sample buffer. Bound material, along with small amount of the input lysates, was separated on 10% SDS–PAGE and transferred onto nitrocellulose membrane. Rab11-3xHA and Snz-GFP were detected by anti-HA-HRP (Roche 12013819001), anti-GFP (Abcam ab6556), and antirabbit-HRP (Sigma A0545) antibodies, respectively, using ECL Prime reagent (Cytiva RPN2232) and x-ray film for detection.

ACKNOWLEDGMENTS

We thank Szilvia Bozsó and Mónika Truszka for technical assistance. We thank Mike W. Henne for suggestions and for providing reagents and Michael Krahn and Thomas L. Schwarz for providing reagents. This work was supported by the National Research Development and Innovation Office (NKFIH) of Hungary with PD135611 grant to T.M., ÚNKP-22-2-III-ELTE-702 grant to D.H., FK138851 grant to P.L., and Elvonal KKP129797 and the National Laboratory of Biotechnology 2022-2.1.1-NL-2022-00008 grants to G.J. The work was also supported by the Eötvös Loránd University Excellence Fund (EKA 2022/045-P101-2) to P.L.. This research work was conducted with additional support from the National Academy of Scientist Education under the sponsorship of the Hungarian Ministry of Innovation and Technology (FEIF/646-4/2021-ITM_SZERZ).

REFERENCES

Akizu N, Cantagrel V, Zaki MS, Al-Gazali L, Wang X, Rosti RO, Dikoglu E, Gelot AB, Rosti B, Vaux KK, *et al.* (2015). Biallelic mutations in SNX14 cause a syndromic form of cerebellar atrophy and lysosome-autophagosome dysfunction. Nat Genet 47, 528–534.

Amatya B, Lee H, Asico LD, Konkalmatt P, Armando I, Felder RA, Jose PA (2021). SNX-PXA-RGS-PXC subfamily of SNXs in the regulation of receptor-mediated signaling and membrane trafficking. Int J Mol Sci 22, 2319.

Atienza-Manuel A, Castillo-Mancho V, Renzis SD, Culi J, Ruiz-Gómez M (2021). Endocytosis mediated by an atypical CUBAM complex modulates slit diaphragm dynamics in nephrocytes. Development 148, 199894.

Bare LA, Morrison AC, Rowland CM, Shiffman D, Luke MM, Iakoubova OA, Kane JP, Malloy MJ, Ellis SG, Pankow JS (2007). Five common gene variants identify elevated genetic risk for coronary heart disease. Genet Med 9, 682–689.

Bechtel W, Helmstädter M, Balica J, Hartleben B, Kiefer B, Hrnjic F, Schell C, Kretz O, Liu S, Geist F (2013). Vps34 deficiency reveals the importance of endocytosis for podocyte homeostasis. J Am Soc Nephrol 24, 727–743.

Bucci C, Parton RG, Mather IH, Stunnenberg H, Simons K, Hoflack B, Zerial M (1992). The small GTPase rab5 functions as a regulatory factor in the early endocytic pathway. Cell 70, 715–728.

Chang C-L, Hsieh T-S, Yang TT, Rothberg KG, Azizoglu DB, Volk E, Liao J-C, Liou J (2013). Feedback regulation of receptor-induced Ca2+ signaling mediated by E-syt1 and Nir2 at endoplasmic reticulum-plasma membrane junctions. Cell Rep 5, 813–825.

Chen KE, Healy MD, Collins BM (2019). Towards a molecular understanding of endosomal trafficking by Retromer and Retriever. Traffic 20, 465–478.

Costantino BFB, Bricker DK, Alexandre K, Shen K, Merriam JR, Antoniewski C, Callender JL, Henrich VC, Presente A, Andres AJ (2008). A novel ecdysone receptor mediates steroid-regulated developmental events during the mid-third instar of Drosophila. PLos Genet 4, e1000102.

Csizmadia T, Lőrincz P, Hegedűs K, Széplaki S, Lőw P, Juhász G (2018). Molecular mechanisms of developmentally programmed crinophagy in *Drosophila*. J Cell Biol 217, 361–374.

Datta S, Liu Y, Hariri H, Bowerman J, Henne WM (2019). Cerebellar ataxia disease-associated Snx14 promotes lipid droplet growth at ER-droplet contacts. J Cell Biol 218, 1335–1351.

Datta S, Bowerman J, Hariri H, Ugrankar R, Eckert KM, Corley C, Vale G, McDonald JG, Henne WM (2020). Snx14 proximity labeling reveals a role in saturated fatty acid metabolism and ER homeostasis defective in SCAR20 disease. Proc Nat Acad Sci USA 117, 33282–33294.

Denholm B, Skaer H (2009). Bringing together components of the fly renal system. Curr Opin Genet Dev 19, 526–532.

Du Y, Zou Y, Yu W, Shi R, Zhang M, Yang W, Duan J, Deng Y, Wang X, Lü Y (2013). Expression pattern of sorting nexin 25 in temporal lobe epilepsy: a study on patients and pilocarpine-induced rats. Brain Res 1509, 79–85.

Feng F, Sun H, Zhao C, Sun C, Zhao Y, Lin H, Yang J, Xiao Y, Wang W, Wu D (2022). Identification of APC mutation as a potential predictor for immunotherapy in colorectal cancer. J Oncol 2022, 6567998.

Formica M, Storaci AM, Bertolini I, Carminati F, Knævelsrud H, Vaira V, Vaccari T (2021). V-ATPase controls tumor growth and autophagy in a Drosophila model of gliomagenesis. Autophagy 17, 4442–4452.

Fu Y, Zhu J-Y, Zhang F, Richman A, Zhao Z, Han Z (2017). Comprehensive functional analysis of Rab GTPases in Drosophila nephrocytes. Cell Tissue Res 368, 615–627.

Gallon M, Cullen PJ (2015). Retromer and sorting nexins in endosomal sorting. Biochem Soc Trans 43, 33–47.

Gillingham AK, Sinka R, Torres IL, Lilley KS, Munro S (2014). Toward a comprehensive map of the effectors of Rab GTPases. Dev Cell 31, 358–373.

Hao X, Wang Y, Ren F, Zhu S, Ren Y, Jia B, Li Y-P, Shi Y, Chang Z (2011). SNX25 regulates TGF-β signaling by enhancing the receptor degradation. Cell Signal 23, 935–946.

Hariri H, Speer N, Bowerman J, Rogers S, Fu G, Reetz E, Datta S, Feathers JR, Ugrankar R, Nicastro D, Henne WM (2019). Mdm1 maintains endoplasmic reticulum homeostasis by spatially regulating lipid droplet biogenesis. J Cell Biol 218, 1319–1334.

Helmstädter M, Huber TB, Hermle T (2017). Using the *Drosophila* nephrocyte to model podocyte function and disease. Front Pediatr 5, 262.

Henne WM, Zhu L, Balogi Z, Stefan C, Pleiss JA, Emr SD (2015). Mdm1/Snx13 is a novel ER-endolysosomal interorganelle tethering protein. J Cell Biol 210, 541–551.

Hochapfel F, Denk L, Mendl G, Schulze U, Maaßen C, Zaytseva Y, Pavenstädt H, Weide T, Rachel R, Witzgall R, Krahn MP (2017). Distinct functions of crumbs regulating slit diaphragms and endocytosis in Drosophila nephrocytes. Cell Mol Life Sci 74, 4573–4586.

Huotari J, Helenius A (2011). Endosome maturation. EMBO J 30, 3481–3500.

Jacques MPC, Baris O, Prunier-Mirebeau D, Savagner F, Rodien P, Rohmer V, Franc B, Guyetant S, Malthiery Y, Reynier P (2005). Two-step differential expression analysis reveals a new set of genes involved in thyroid oncocytic tumors. J Clin Endocrinol Metab 90, 2314–2320.

Kampf LL, Schneider R, Gerstner L, Thünauer R, Chen M, Helmstädter M, Amar A, Onuchic-Whitford AC, Munarriz RL, Berdeli A, *et al.* (2019). *TBC1D8B* mutations implicate Rab11-dependent vesicular trafficking in the pathogenesis of nephrotic syndrome. J Am Soc Nephrol 30, 2338–2353.

Kim HR, Jin HS, Eom YB (2021). Metabolite genome-wide association study for indoleamine 2,3-dioxygenase activity associated with chronic kidney disease. Genes 12, 1905.

Kosaka T, Ikeda K (1983). Reversible blockage of membrane retrieval and endocytosis in the garland cell of the temperature-sensitive mutant of Drosophila melanogaster, shibirets1. J Cell Biol 97, 499–507.

Lauzier A, Bossanyi M-F, Larcher R, Nassari S, Ugrankar R, Henne WM, Jean S (2022). Snazarus and its human ortholog SNX25 modulate autophagic flux. J Cell Sci 135, jcs258733.

Li J, Li C, Zhang D, Shi D, Qi M, Feng J, Yuan T, Xu X, Liang D, Xu L, *et al.* (2014). SNX13 reduction mediates heart failure through degradative sorting of apoptosis repressor with caspase recruitment domain. Nat Commun 5, 5177.

Lőrincz P, Lakatos Z, Varga Á, Maruzs T, Simon-Vecsei Z, Darula Z, Benkő P, Csordás G, Lippai M, Andó I, *et al.* (2016). MiniCORVET is a Vps8-containing early endosomal tether in Drosophila. eLife 5, e14226.

Lund VK, Madsen KL, Kjaerulff O (2018). Drosophila Rab2 controls endosome-lysosome fusion and LAMP delivery to late endosomes. Autophagy. 14, 1520–1542.

Ma C-I, Yang Y, Kim T, Chen CH, Polevoy G, Vissa M, Burgess J, Brill JA (2020). An early endosome-derived retrograde trafficking pathway promotes secretory granule maturation. J Cell Biol 219, e201808017.

Milosavljevic J, Lempicki C, Lang K, Heinkele H, Kampf LL, Leroy C, Chen M, Gerstner L, Spitz D, Wang M, *et al.* (2022). Nephrotic syndrome gene TBC1D8B is required for endosomal maturation and nephrin endocytosis in Drosophila. J Am Soc Nephrol 33, 2174–2193.

Murthy M, Garza D, Scheller RH, Schwarz TL (2003). Mutations in the exocyst component Sec5 disrupt neuronal membrane traffic, but neurotransmitter release persists. Neuron 37, 433–447.

Naslavsky N, Caplan S (2018). The enigmatic endosome - sorting the ins and outs of endocytic trafficking. J Cell Sci 131, jcs216499.

Neuman SD, Lee AR, Selegue JE, Cavanagh AT, Bashirullah A (2021). A novel function for Rab1 and Rab11 during secretory granule maturation. J Cell Sci 134, jcs259037.

Olsson AH, Volkov P, Bacos K, Dayeh T, Hall E, Nilsson EA, Ladenvall C, Rönn T, Ling C (2014). Genome-wide associations between genetic and epigenetic variation influence mRNA expression and insulin secretion in human pancreatic islets. PLos Genet 10, e1004735.

Paschinger K, Rendić D, Wilson IBH (2009). Revealing the anti-HRP epitope in Drosophila and Caenorhabditis. Glycoconj J 26, 385–395.

Paul B, Weeratunga S, Tillu VA, Hariri H, Henne WH, Collins BM (2022). Structural predictions of the SNX-RGS proteins suggest they belong to a new class of lipid transfer proteins. Front Cell Dev Biol 10, 826688.

Satoh AK, O'Tousa JE, Ozaki K, Ready D (2005). Rab11 mediates post-Golgi trafficking of rhodopsin to the photosensitive apical membrane of Drosophila photoreceptors. Development 132, 1487–1497.

Suh JM, Stenesen D, Peters JM, Inoue A, Cade A, Graff JM (2008). An RGS-containing sorting nexin controls Drosophila lifespan. PLoS One 3, e2152.

Tanaka T, Nakamura A (2008). The endocytic pathway acts downstream of Oskar in Drosophila germ plasm assembly. Development 135, 1107–1117.

Teasdale RD, Collins BM (2012). Insights into the PX (phox-homology) domain and SNX (sorting nexin) protein families: structures, functions and roles in disease. Biochem J 441, 39–59.

Thomas AC, Williams H, Setó-Salvia N, Bacchelli C, Jenkins D, O'Sullivan M, Mengrelis K, Ishida M, Ocaka L, Chanudet E, *et al.* (2014). Mutations in SNX14 cause a distinctive autosomal-recessive cerebellar ataxia and intellectual disability syndrome. Am J Hum Genet 95, 611–621.

Ugrankar R, Bowerman J, Hariri H, Chandra M, Chen K, Bossanyi M-F, Datta S, Rogers S, Eckert KM, Vale G, *et al.* (2019). Drosophila snazarus regulates a lipid droplet population at plasma membrane-droplet contacts in adipocytes. Dev Cell 50, 557–572.e5.

Vecellio M, Paraboschi AC, Isailovic N, Motta F, Cardamone G, Robusto M, Asselta R, Brescianini S, Sacrini F, Costanzo A, *et al*. (2021). DNA methylation signature in monozygotic twins discordant for psoriatic disease. Front Cell Dev Biol 9, 778677.

Weavers H, Prieto-Sánchez S, Grawe F, Garcia-López A, Artero R, Wilsch-Bräuninger M, Ruiz-Gómez M, Skaer H, Denholm B (2009). The insect nephrocyte is a podocyte-like cell with a filtration slit diaphragm. Nature 457, 322–326.

Welz T, Wellbourne-Wood J, Kerkhoff E (2014). Orchestration of cell surface proteins by Rab11. Trends Cell Biol 24, 407–415.

Wen P, Zhang F, Fu Y, Zhu J-Y, Han Z (2020). Exocyst genes are essential for recycling membrane proteins and maintaining slit diaphragm in Drosophila nephrocytes. J Am Soc Nephrol 31, 1024–1034.

Zhou C, Wu Z, Du W, Que H, Wang Y, Ouyang Q, Jian F, Yuan W, Zhao Y, Tian R (2022). Recycling of autophagosomal components from autolysosomes by the recycler complex. Nat Cell Biol 24, 497–512.

Zhuang S, Shao H, Guo F, Trimble R, Pearce E, Abmayr SM (2009). Sns and Kirre, the Drosophila orthologs of Nephrin and Neph1, direct adhesion, fusion and formation of a slit diaphragm-like structure in insect nephrocytes. Development 136, 2335–2344.